BMC Biology

RESEARCH ARTICLE Open Access

Hoxa5 alleviates adipose tissue metabolic distortions in high-fat diet mice associated with a reduction in MERC

Qi Chen[1], Zeyu Ren[1], Liping Dang[1], Zunhai Liu[1], Simeng Wang[1], Xinhao Chen[1], Guiping Qiu[1] and Chao Sun[1*]

Abstract

Background Mitochondria-endoplasmic reticulum membrane contact (MERC) is an important mode of intercellular organelle communication and plays a crucial role in adipose tissue metabolism. Functionality of Hoxa5 is an important transcription factor involved in adipose tissue fate determination and metabolic regulation, but the relationship between Hoxa5 and MERC is not well understood.

Results In our study, we established an obesity model mouse by high-fat diet (HFD), induced the alteration of Hoxa5 expression by adenoviral transfection, and explored the effect of Hoxa5 on MERC dysfunction and metabolic distortions of adipose tissue with the help of transmission electron microscopy, calcium ion probe staining, and other detection means. The results showed Hoxa5 was able to reduce MERC production, alleviate endoplasmic reticulum stress (ERS) and calcium over-transport, and affect cGAS-STING-mediated innate immune response affecting adipose tissue energy metabolism, as well as affect the AKT-IP3R pathway to alleviate insulin resistance and ameliorate metabolic distortions in adipose tissue of mice.

Conclusions Our results suggest that Hoxa5 can ameliorate high-fat diet-induced MERC overproduction and related functional abnormalities, in which finding is expected to provide new ideas for the improvement of obesity-related metabolic distortions.

Keywords Hoxa5, Mitochondria-endoplasmic reticulum membrane contact (MERC), Calcium ion homeostasis

Introduction

Obesity presents a significant health challenge in contemporary society and has become a critical measure of the effectiveness of the global public health system. Typically, obesity is correlated with other chronic conditions, including diabetes, cardiovascular disease, and non-alcoholic fatty liver disease [1]. Unhealthy dietary habit is a contributing factor to obesity, and the consumption of high-calorie diets has resulted in a noteworthy escalation in obesity rates.

The Homeobox (Hox) gene is a highly conserved superfamily of regulatory genes characterized by the inclusion of the Homebox sequence consisting of 183 nucleotide sequences [2]. Due to the highly conserved nature of Hox family genes and the temporal and spatial characteristics of their expression, they are closely related to the development process of organisms and are important transcription factors that play important roles in cell proliferation, differentiation, apoptosis, and organ development [3, 4]. *Hoxa5*, a crucial member of the Hox gene family, plays a significant role in adipose tissue expansion and fate determination [5]. *Hoxa5* promotes adipose differentiation by increasing DNA methylation levels and

*Correspondence:
Chao Sun
sunchao2775@163.com
[1] College of Animal Science and Technology, Northwest A&F University, No. 22 Xi Nong Roud, Yangling 712100, Shaanxi, China

inhibiting the PKA/HSL signaling pathway in mice, it also reduces endoplasmic reticulum stress and promotes the polarization of M2 macrophages, leading to alleviation of obesity-induced adipose tissue inflammation [6]. Furthermore, the expression of *Hoxa5* gene is linked to the proliferation and differentiation of brown adipose tissue and skeletal muscle cells [7]. Whole-genome sequencing of mice that were fed a HFD revealed that the *Hoxa5* gene underwent changes in DNA methylation and transcriptional repression in adipose tissue [8]. In response to metabolic distortions induced by high-fat diets, these findings suggest that *Hoxa5* may occur to play a key role in metabolic regulation.

The endoplasmic reticulum (ER) and mitochondria are involved in the synthesis, transportation, and metabolism of protein and lipid in cells, form contacts in time and space, and coordinate with each other functionally to control intracellular calcium signaling transmission and lipid exchange and maintain cellular metabolic homeostasis [9, 10]. The membrane structure of the ER in contact with mitochondria is known to have been clearly isolated and identified only in the 1990s, which was named mitochondria-associated membrane (MAM), also known as mitochondria-endoplasmic reticulum membrane contact (MERC) [11]. MERC has strong plasticity and participates in a variety of life activities. It is considered necessary for phospholipid transmembrane transport and Ca^{2+} transfer to mitochondria and participates in the activation of tricarboxylic acid cycle (TCA cycle) [12–14]. ACAT1 localized on MERC can also catalyze the formation of cholesteryl esters from free cholesterol, thus controlling the balance between membrane cholesterol and free cholesterol [15]. Research has shown that lack of MERC integrity leads to metabolic abnormalities such as mitochondrial dysfunction, endoplasmic reticulum stress, and insulin resistance [16, 17].

We have previously determined that *Hoxa5* plays a role in regulating adipocyte proliferation and metabolism [18]. However, it is still unclear whether *Hoxa5* can affect lipid and energy metabolism through the MERC structure of adipocytes. Therefore, our study was conducted to investigate the effect of *Hoxa5* on the structure and function of MERC in adipocytes and further explore the pathways by which *Hoxa5* regulates energy metabolism and insulin resistance in adipose tissue, so as to provide novel insights for illuminating the energy metabolic network of adipose tissue.

Methods

Adenoviral vector construction

Based on the CDs (coding sequence) of the Hoxa5 gene (*Mus musculus*) in NCBI, amplification primers were designed using Primer 6.0 (Hoxa5-F: ATTCCACTTCAA CCGCTAC; Hoxa5-R: TCCACTTCATCCTCCTGTT), and Kpn I and Xho I cleavage sites with protected bases were added to both ends of the primers. Afterwards, the CDs region was amplified, and the CDs were ligated to the double digest product of pAdTrack-CMV overnight at 16 °C under the action of T4DNA ligase (TaKaRa). The product was transfected into E.coli DH5α receptor cells, and the pAdTrack-CMV-Hoxa5 shuttle plasmid was identified after plasmid extraction. The recombinant plasmid was linearized by Pme I digestion for 4 h. The gel recovery product was dephosphorylated by CIAP for 1 h. After ethanol precipitation, the recombinant plasmid was transformed into 100 μl of BJ5183 receptor cells containing pAdEasy-1 backbone vector for homologous recombination at 1 μg, and then the plasmid was extracted for enzyme digestion and PCR identification.

After that, the constructed adenoviral vector was linearized by Pac I digestion, purified using ethanol precipitation, and transferred into 293A cells for viral packaging. Finally, 293A cells were infiltrated using the viral stock solution, and fluorescence expression was observed after 24 h. Cells were collected after 48 h. After repeated freeze–thaw lysis, the supernatant was collected to repeat the infiltration of 293A cells for enrichment and purification, and the resultant viral vectors were tested for titer by 293 T cells.

The interfering fragments used in the experiments were designed based on BLOCK-iTTM RNAi Designer (Invitrogen) with the following sequences (top: CACCGCACA TTAGTCACGACAATATCTCGAGATATTGTCGTG ACTAATGTGC; bottom: AAAAGCACATTAGTCACG ACAATATCTCGAGATATTGTCGTGACTAATGTGC), and Kpn I and Xho I cleavage sites with protected bases were added to both ends of the primers. The subsequent adenoviral vector construction process is similar.

Animal experiment

All experimental animals were housed in environmentally controlled chambers (temperature: 25℃ ± 1℃; humidity: 55% ± 5%; 12-h light/dark cycle) and all animals fed ad libitum. Four-week-old male C57BL/6 mice purchased from the Experimental Animal Center of Air Force Medical University (Xi'an, Shaanxi Province) were acclimatized and fed for 2 weeks. Afterwards, the mice were divided into two groups at random and fed either a normal diet (Chow) or a high-fat diet (HFD: with fat contributing to 60% of the total energy intake) for a period of 10 weeks to induce obesity. And at the end of the tenth week, the relevant indexes were tested to determine the completion of mold making. Following this, the mice in the high-fat diet group were divided into three groups at random and were intraperitoneal injected with purified products of adenoviral vectors overexpressing

Hoxa5 (pAd-*Hoxa5*), interfering adenoviral vectors of *Hoxa5* (sh-*Hoxa5*), or unloaded adenoviral vectors (pAd-Control) at a titer of 1×10^{10} IFU/mL for a duration of 3 weeks. Meanwhile, some of the Chow as well as HFD group mice were kept and continued to be fed for 3 weeks, a total of 13 weeks. Mice were euthanized by cervical dislocation after overnight fasting and anesthesia with isoflurane (2%), subcutaneous white adipose tissue, inguinal white adipose tissue, and serum samples were collected. The collected tissue samples were rinsed with saline, weighed, immediately frozen in liquid nitrogen, and stored at − 80 °C.

Primary adipocyte culture

White inguinal adipose tissue was collected from 4-week-old mice, and then visible fibers and blood vessels were removed. It was then washed three times with PBS buffer, clipped, and digested using collagenase, followed by filtration using a filter membrane, centrifugation, and resuspension using a culture medium. Primary preadipocytes were seeded at a density of 30% in culture dishes and maintained in a humidified environment at 37℃, 5% CO_2. To induce differentiation of preadipocytes, cells were cultured in DMEM/F12 medium supplemented with dexamethasone (1 μmol/L; Sigma), insulin (1 μg/mL; Sigma), IBMX (0.5 mmol/L; Sigma), and 10% fetal bovine serum until they reached 100% confluence (day 0). Subsequently, cells were maintained in an induction medium containing insulin (1 μg/mL; Sigma) and 10% fetal bovine serum from day 2 to day 4 after induction. Primary adipocytes were infected for 48 h in this procedure using an overexpressed *Hoxa5* adenoviral vector (pAd-*Hoxa5*) or an adenoviral interference vector for *Hoxa5* (sh-*Hoxa5*) at a dose of 1×10^{9} IFU/mL, with a null vector (pAd-Control) as a control.

Isolation and extraction of MERC

The mice underwent overnight fasting prior to euthanasia, and 1 g of inguinal adipose tissue was promptly collected and weighed after dissection. The tissue was then washed three times in pre-chilled Buffer I, finely minced, and immersed in Buffer II. After being filtered, the sample was then transferred to a glass vessel containing 30 mL of Buffer I and further fragmented via homogenization. The homogenate was centrifuged at 740 × g for 5 min, and this process was repeated twice to obtain the supernatant. This was followed by centrifugation at 8000 × g for 10 min and repeated three times to collect the precipitate (crude mitochondrial fraction), while the supernatant was kept to collect the ER fraction. The crude mitochondrial preparation was layered over buffer III containing a 30% Percoll gradient and subjected to ultracentrifugation at 95,000 × g for 30 min. As a result, the pure mitochondrial fraction was pelleted at the bottom of the tube, while an intermediate layer containing MERC was formed between the supernatant and the pure mitochondrial fraction. The MAM fractions were then collected and diluted ten times in MRB buffer for subsequent experiments.

(Buffer I: mannitol 225 mM, sucrose 75 mM, Tris–HCl 30 mM, BSA 0.5% and EGTA 0.5 mM, pH 7.4. Buffer II: mannitol 225 mM, sucrose 75 mM, Tris–HCl 30 mM, BSA 0.5%, pH 7.4. Buffer III: mannitol 225 mM, sucrose 75 mM, Tris–HCl 30 mM, pH 7.4. MRB buffer: mannitol 225 mM, Hepes 5 mM, EGTA 0.5 mM, pH 7.4).

Transmission *electron* microscopy (TEM) sample preparation

Inguinal white adipose tissue was collected from mice in the Chow and HFD groups, and tissue fragments of approximately 1 mm^3 in size were clipped. The tissue was subsequently fixed for 5 h at 4 °C using a fixative solution comprising of 2.5% glutaraldehyde, which was prepared in phosphate buffer (0.1 M, pH 7.2–7.4). The samples were rinsed three times with PBS phosphate buffer for 15 min each, followed by the addition of 1% osmium acid for 2 h. The samples were rinsed three times with PBS phosphate buffer for 10 min each, followed by dehydration with 30%, 50%, 70%, 80%, 90%, and 100% ethanol, twice per gradient for 8 min each. This was followed by infiltration treatment with 25% LR-White (diluted with anhydrous ethanol) for 2 h, 50% pure embedding agent for 8 h, 75% embedding agent for 12 h, and 100% pure embedding agent twice for 24 h each. After embedding using embedding molds, the capsules were polymerized in a 55℃ oven for 48 h. The polymerized capsule samples were trimmed into tower-shaped spikes using a block trimmer. The samples were stained with 2% uranyl acetate for 10–30 min or lead citrate for 5–15 min, dried, and ready for observation by transmission electron microscopy.

Immunoblotting analyses

Proteins were extracted from tissues and cells with the assistance of a lysis buffer (Solarbio, Beijing, China), based on prior laboratory investigations [19]. Approximately 30 μg of proteins were separated using electrophoresis on 12% and 5% SDS-PAGE gels, and then transferred onto PVDF nitrocellulose membranes (Millipore, MA, USA). The membranes were blocked for 2 h using 5% skim milk in Tris-Tween buffer, incubated overnight at 4℃ with primary antibody, followed by incubation with HRP-conjugated secondary antibodies (Abcam, Cambridge, UK) for 2 h. Finally, the proteins were visualized using a chemiluminescent peroxidase substrate from Millipore (Massachusetts, USA) and quantified using a

ChemiDoc XRS system from Bio-Rad (Richmond, CA, USA). All immunoblot analyses were performed using GAPDH (36 kDa) as an internal reference, and relative levels were calculated based on the Chow/pAd-Control group.

Quantitative real-time PCR

RNA was extracted from tissues and cells for reverse transcription to cDNA at an amount of 500 ng RNA per system (TRI Pure Reagent Kit and M-MLV Reverse Transcriptase Kit, Takara, Dalian, China). Primers were designed based on mouse gene sequences and synthesized by Invitgen (Shanghai, China). RT-qPCR was performed in a 20 μL reaction system containing specific primers and SYBR premixes (Vazyme Biotech, Nanjing, China). Amplification was performed using an ABI StepOne plus RT-PCR system (Carlsbad, CA). Gene mRNA expression levels were analyzed using the $2^{-\Delta\Delta Ct}$ method using β-actin as reference gene. All RT-qPCR programs were performed using SYBR® Green dye with β-actin as an internal reference and relative values were calculated based on Chow/pAd-Control group.

Glucose tolerance test (GTT) and insulin tolerance test (ITT)

Glucose tolerance test: after fasting for 16 h, mice were injected intraperitoneally with glucose (1.5 g/kg). The tail vein blood glucose levels were measured before injection (0 min) and 15, 30, 45, 60, 90, and 120 min after injection using an ACCU-CHEK® Performa glucometer (Roche Diabetes Care GmbH, Mannheim, Germany). Insulin tolerance test: the insulin sensitivity of mice was measured by intraperitoneal insulin injection (0.4 U/kg) into fasted mice for 5 h, after which changes in blood glucose levels in the tail vein of mice were detected by the same method as above.

Immunofluorescence

Cells were treated according to the experimental requirements and fixed with 4% formalin salt solution, then closed with phosphate buffer containing 5% BSA for 1 h at room temperature, followed by incubation with rabbit-derived NRF2 primary antibody overnight at 4℃, then incubated with isothiocyanate fluorescein-coupled goat anti-rabbit lgG secondary antibody for 1 h at room temperature, and then the nuclei were stained with DAPI for 5 min. Observational photographs were taken using a Cytation3 Cell Imaging Multi-Mode Reader (BioTek, Winooski, VT, USA).

Ca^{2+} fluorescence staining

Calcium ion probe Fluo-3, AM (Solarbio, Beijing, China) is one of the most commonly used fluorescent probes for the detection of intracellular calcium ion concentration. Dilute the reservoir solution with HBSS buffer and prepare 1–5 μM of Fluo-3, AM working solution. Remove the medium and wash the cells three times with HBSS. Remove the buffer, cover the cells with Fluo-3, AM working solution, and incubate at 37 °C for 20 min. Remove the working solution and wash the cells three times with buffer. Add HBSS solution containing 1% fetal bovine serum to cover the cells and incubate the cells in a cell culture incubator at 37 °C for 40 min. Wash the cells appropriately with buffer and observe the cells with an inverted fluorescence microscope with an excitation wavelength of 480–500 nm and an emission wavelength of 525–530 nm.

Mitochondrial calcium level assay

According to the kit instructions, configure the Mediator Solution (Reagent C) and the Staining Solution (Reagent B) as the staining working solution; 100 μL of diluted purified mitochondrial solution, Reagent D, and Reagent E were added to the 96-well plate, respectively. Afterwards, 10 μL of staining working solution was added to each well, mixed well and subsequently incubated at 22 °C for 30 min, placed at 37 °C for 30 min, and then detected using a fluorescent enzyme marker (excitation wavelength 550 nm) to calculate the concentration of mitochondrial calcium ions.

Data analysis

Statistical analysis of data differences was performed using GraphPad Prism 6.0 software. Data were compared using the *t*-test to analyze whether there was a significant difference between the two groups; data were compared in multiple groups using one-way or two-way analysis of variance (ANOVA) followed by the Bonferroni test. Data are expressed as mean ± standard deviation (mean ± SD). $^{*}p < 0.05$, $^{**}p < 0.01$ were considered to indicate statistical significance.

Results

Hoxa5 inhibits the formation of MERC induced by high-fat diet

Long-term high-fat diet can lead to distortions of lipid metabolism and various metabolic diseases in the organism. We constructed an obese mouse model by feeding high-fat diets (HFD) and measured the levels of serum triglycerides and free fatty acids (FFAs) as well as the expression levels of lipid metabolism-related genes in subcutaneous white adipose tissue and found that the obese model mice showed significant distortions of lipid metabolism (Additional file 1: Fig.S1 A-C).

MERC structures as sites of physical contact between the endoplasmic reticulum and mitochondria mediated by proteins play a critical role in both energy and lipid

metabolism. Therefore, we studied the effect of HFD on the generation of MERC and assessed the close contact of mitochondria with the ER membrane. We collected inguinal white adipose tissue (iWAT) from mice in the Chow and HFD groups and prepared ultra-thin sections for examination using transmission electron microscopy, and statistic of the ratio of mitochondria in close contact with the ER to the total number of mitochondria was counted, and relative levels were calculated using the Chow group as a standard. The results showed that there was a significant increase ($p < 0.05$) in the contact between mitochondria and endoplasmic reticulum in mice in the HFD group (Fig. 1A). The structure formation of MERC depends on the interaction of membrane proteins of the mitochondria with the ER, while its function depends on the action of a series of regulatory proteins, resulting in a dynamic structure that communicates with each other without membrane fusion [20]. Therefore, we examined the expression levels of MERC-related proteins such as STING, PACS-2, Sigma-1R and Mfn-2, and found that the expression changes were consistent with the TEM results (Fig. 1 B, C), which laterally indicated that HFD led to an increase in MERC production.

We further explored the intrinsic mechanism causing the changes in MERC and observed that along with the increased generation of MERC structures, the levels of Hoxa5 protein as well as mRNA expression in iWAT produced a downregulation (Additional file 1: Fig.S1 D, E). Therefore, we hypothesized that MERC formation might be regulated by Hoxa5, for which we constructed the overexpressing *Hoxa5* adenovirus vectors (pAd-*Hoxa5*) and interfering *Hoxa5* adenovirus vectors (sh-*Hoxa5*), and injected them intraperitoneally into high-fat mice, and detected variations in the expression levels of *Hoxa5* in iWAT, Liver, eWAT, and BAT (Additional file 1: Fig.S1 F–H). We found that overexpression of Hoxa5 reduced MERC in iWAT of mice and interference with Hoxa5 resulted in the opposite result (Fig. 1 D). Similarly, the marker proteins of MERC and the expression of

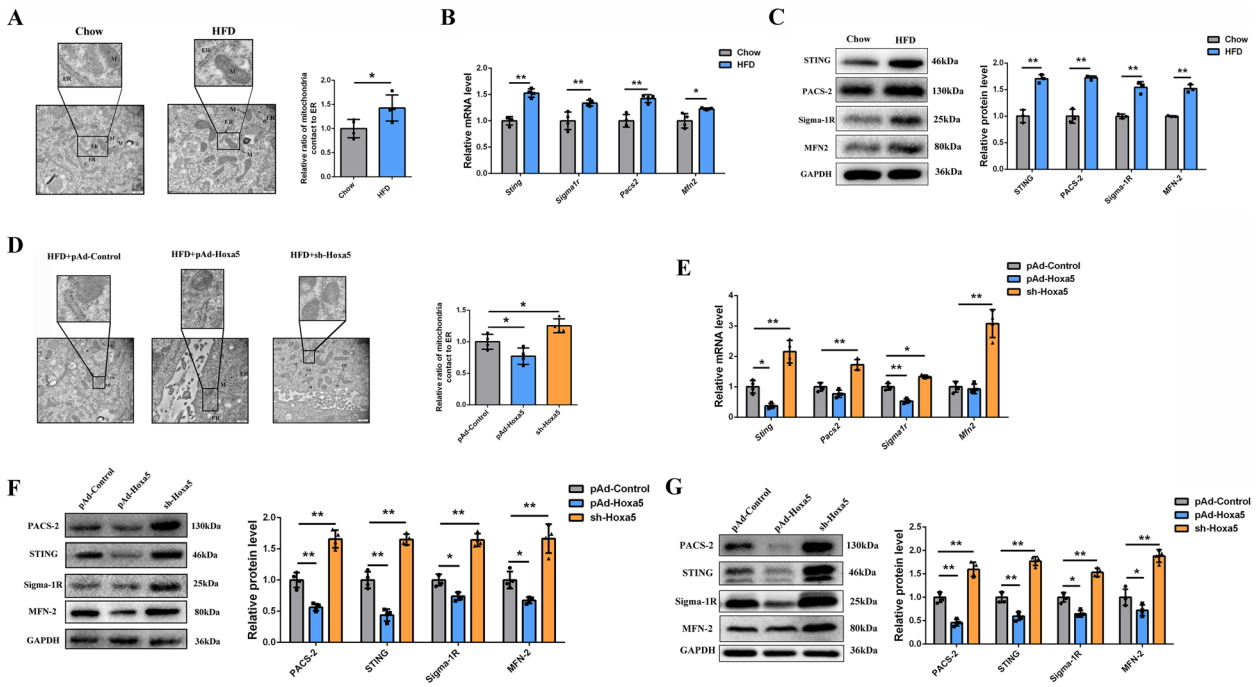

Fig. 1 Hoxa5 inhibits the formation of MERC induced by high-fat diet. **A** iWAT was collected from Chow and HFD groups, observed by TEM, and mitochondrial contact with the ER was counted. **B** iWAT was collected from Chow and HFD groups, *Sting*, *Sigma1r*, *Pacs2*, and *Mfn2* were quantified using RT-qPCR. **C** iWAT was collected from mice in Chow and HFD groups, and immunoblotting analysis was performed on STING (46 kDa), PACS-2 (130 kDa), Sigma-1R (25 kDa), and MFN-2 (80 kDa). **D** After overexpression/disruption of Hoxa5 in the HFD group, iWAT was collected and observed using transmission electron microscopy, and mitochondrial contact with the ER was counted. **E** iWAT was collected from each group after overexpression/interference of *Hoxa5*, *Sting*, *Sigma1r*, *Pacs2*, and *Mfn2* were quantified using RT-qPCR. **F** iWAT was collected from each group after overexpression/interference of *Hoxa5*, immunoblotting analysis was performed on STING (46 kDa), PACS-2 (130 kDa), Sigma-1R (25 kDa), and MFN-2 (80 kDa). **G** After enrichment of the MERC fraction, immunoblotting analysis was performed on STING (46 kDa), PACS-2 (130 kDa), Sigma-1R (25 kDa), and MFN-2 (80 kDa) in each group of MERC fraction. $n = 4$ in each group, values are mean ± SD. *$p < 0.05$, **$p < 0.01$. iWAT inguinal white adipose tissue, HFD high fat diet, TEM transmission electron microscope, ER endoplasmic reticulum, MERC mitochondria endoplasmic reticulum membrane contact

the corresponding genes produced significant changes. ($p < 0.05$) (Fig. 1E, F).

The MERC fraction from adipocytes was further collected using differential centrifugation and the levels of ER protein PACS-2 and mitochondrial protein VDAC were detected in each fraction, which showed that the MERC fraction was of a high purity (Additional file 1: Fig. S1 I). Under minimizing the effect of non-MERC components, we re-examined the changes in the levels of MERC marker proteins, and it was seen that overexpression of Hoxa5 led to a significant reduction in the expression levels of MERC constituent proteins in obese mice, whereas the opposite was true for interference with Hoxa5 (Fig. 1 G).

Hoxa5 alleviates MERC-associated ER stress and Ca^{2+} homeostasis disruption

Although MERC is considered a key structure in energy metabolism and promotes cell adaptation to environmental changes, the presence of excessive MERC is harmful. Studies have shown that increased ER-mitochondrial coupling can promote mitochondrial respiration and bioenergetic synthesis during the early stages of ER stress, but prolonged ER stress can result in extreme metabolic distortions [21]. Therefore, we further explored whether the high-fat diet-induced increase in MERC production leads to the generation of ER stress and probed the role of *Hoxa5*.

MERC structure is closely related to ER stress as an essential platform for ER stress generation and transduction [22, 23]. Thus, we examined the mRNA expression levels of ER stress-related proteins GRP78, CHOP, and IRE1α in mouse iWAT and found that HFD led to a significant increase in the expression levels of ER stress marker proteins ($p < 0.05$) (Fig. 2A). In addition, we examined the levels of ER stress proteins in the enriched MERC fractions (Fig. 2B), further confirming that the increase in MERCs induced by a high-fat diet may cause ER stress to occur. Moreover, overexpression of *Hoxa5* led to a significant reduction in the expression of GRP78, CHOP, and IRE1α in iWAT and MERC fraction, effectively alleviating ER stress, whereas interference with *Hoxa5* expression produced the opposite effect ($p < 0.05$) (Fig. 2C, D). Therefore, we hypothesized that Hoxa5 could reduce the occurrence of ER stress by decreasing MERC generation.

The opening of IP3R channels in the ER membrane under the stimulation of ER stress leads to a large amount of Ca^{2+} efflux, and MERC also plays an important role in this process and participates in the transport of Ca^{2+} [24]. Thus, we further explored the impaired calcium homeostasis that may be caused by MERC abnormalities and ER stress and the effect of *Hoxa5* on it. Our results indicate that a high-fat diet leads to significantly increased mRNA expression levels of *Ip3r1* in mice iWAT ($p < 0.01$) (Additional file 1: Fig.S1 J). Meanwhile, the high-fat diet also led to a significant increase in the protein level of IP3R1 in the enriched MERC fractions (Fig. 2E). In addition, we established a high-fat model by treating primary mouse adipocytes with palmitic acid (0.5 mM for 24 h) and detected intracellular Ca^{2+} concentrations using Ca^{2+} fluorescent probe. The results showed that the concentration of Ca^{2+} in cytoplasm increased significantly after treatment, indicating that high-fat induction may have affected MERC-mediated calcium homeostasis (Fig. 2F). Overexpression of *Hoxa5* significantly reduced the mRNA expression level of *Ip3r1* in iWAT, as well as reduced the protein level of IP3R1 in the enriched MERC fractions, whereas interference with *Hoxa5* appeared to exacerbate the expression of IP3R1 ($p < 0.05$) (Additional file 1: Fig.S1 K, Fig. 2 G). Likewise, we observed that the overexpression of *Hoxa5* considerably diminished the fluorescence intensity of intracellular Ca^{2+}, whereas interference with Hoxa5 increased cytoplasmic Ca^{2+} levels (Fig. 2 H). We also observed in vitro experiments that palmitic acid treatment led to an increase in the expression level of ER stress markers, while overexpression of Hoxa5 could reduce the occurrence of ER stress, and interference with Hoxa5 was the opposite (Additional file 1: Fig.S1 L, M).

Hoxa5 inhibits activation of cGAS-cGAMP-STING pathway induced by high-fat diet

STING, is triggered by its upstream effector, Cyclic GMP-AMP synthase (cGAS), in response to specific activation by double-stranded DNA (dsDNA), which initiates innate immune action [25]. It has been shown that STING is predominantly located on the ER, particularly enriched in the MERC region [26], and is affected by Ca^{2+} concentration, and its unique subcellular localization also permits STING to respond rapidly to alert signals generated by the mitochondria and ER [27].

Obesity induced by a high-fat diet is frequently accompanied by the development of chronic inflammation, as well as impairment of mitochondrial function, and the resulting mtDNA spillover can cause activation of the cGAS-STING pathway [28, 29]. We hypothesized that high-fat diet activates STING-mediated innate immune responses and is influenced by MERC levels. Therefore, changes in cGAS and STING levels in iWAT from mice on a high-fat diet were assessed and HFD was found to cause a significant increase in the levels of both ($p < 0.05$) (Fig. 3A, B). After that, we further examined the effect on cGAS-STING pathway after overexpressing/interfering with *Hoxa5* on HFD group mice and found that mRNA and protein levels of cGAS and STING were significantly

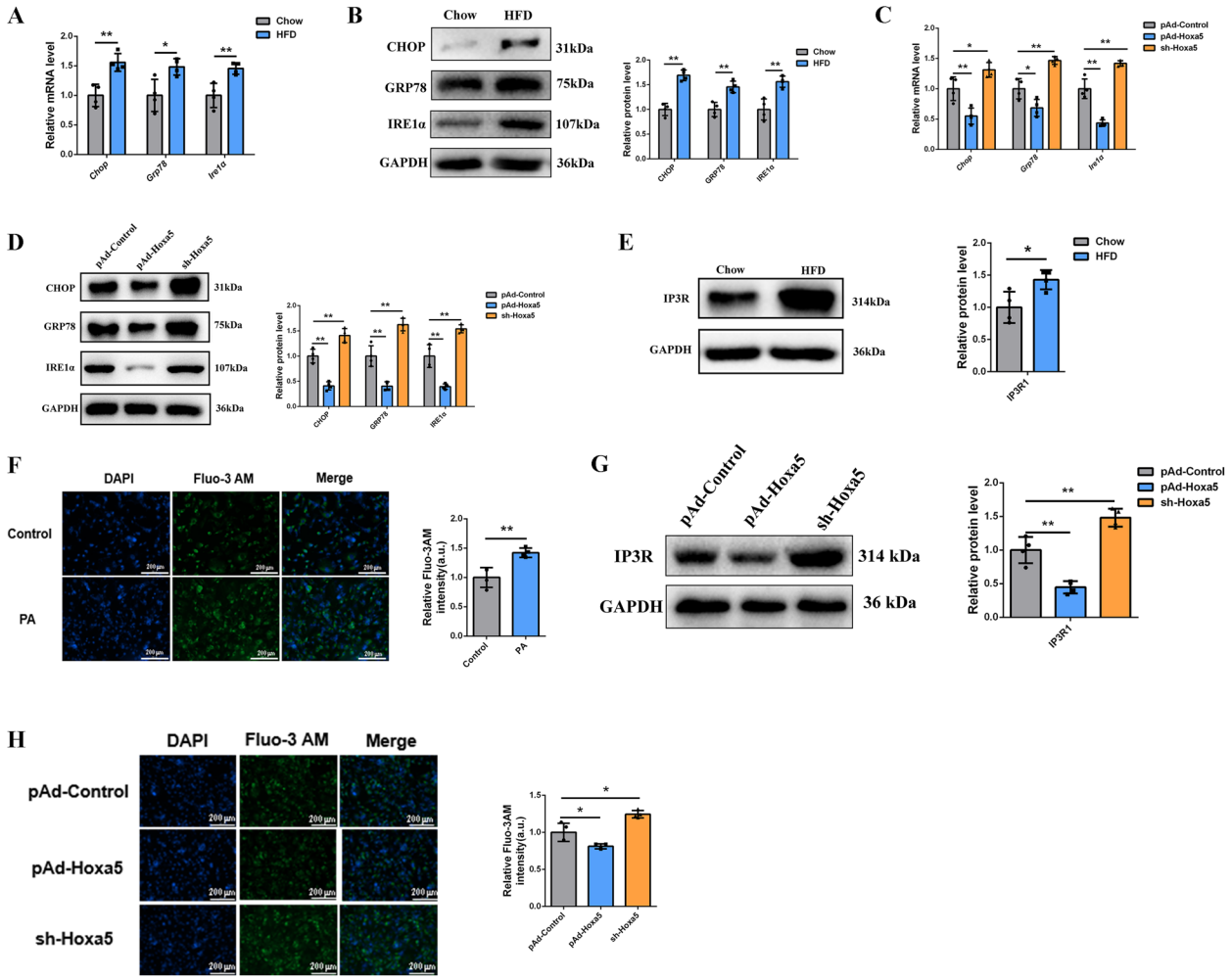

Fig. 2 Hoxa5 alleviates MERC-associated ER stress and Ca2 + homeostasis disruption. **A** iWAT was collected from mice in Chow and HFD groups, *Chop*, *Grp78*, and *Ire1a* were quantified using RT-qPCR; **B** After enrichment of the MERC fraction, immunoblotting analysis was performed on GRP78 (75 kDa), CHOP (31 kDa), and IRE1α (107 kDa). **C** iWAT was collected from each group of mice after overexpression/interference of *Hoxa5* using adenovirus, *Chop*, *Grp78*, and *Ire1a* were quantified using RT-qPCR. **D** After overexpression/interference of *Hoxa5* and enrichment of the MERC fraction, immunoblotting analysis was performed on GRP78 (75 kDa), CHOP (31 kDa), and IRE1α (107 kDa). **E** After enrichment of the MERC fraction, immunoblotting analysis was performed on IP3R1 (314 kDa) in Chow and HFD groups.**F** After treatment of mouse primary adipocytes with palmitic acid, the cells were stained with Fluo-3, AM Calcium probe and observed using IFM. **G** After overexpression/interference of *Hoxa5* and enrichment of the MERC fraction, immunoblotting analysis was performed on IP3R1 (314 kDa). **H** Mouse primary adipocytes were treated with palmitic acid after overexpression/interference of Hoxa5, stained with Fluo-3, AM Calcium probe. $n = 4$ in each group. Values are mean ± SD. *$p < 0.05$, **$p < 0.01$. iWAT inguinal white adipose tissue, HFD high-fat diet, MERC mitochondria–endoplasmic reticulum membrane contact, IFM inverted fluorescence microscope

reduced after overexpressing *Hoxa5*; while interfering with *Hoxa5* led to the opposite result ($p < 0.05$) (Fig. 3C, D). Also, we have demonstrated that the level of STING in the enriched MERC fractions of adipose tissue also changed significantly with the level of Hoxa5 ($p < 0.05$) (Fig. 1G). As can be seen, changes in STING, an important functional protein of MERC, appear to be influenced by MERC formation and are also accompanied by cGAS activation, which may be due to mitochondrial and ER stress.

To further confirm the effect of *Hoxa5* on the cGAS-STING pathway, we conducted overexpression and interference experiments on mouse primary adipocytes and exposed them to palmitic acid (0.5 mM for 24 h) to simulate a high-fat environment. The results demonstrated that overexpression of *Hoxa5* significantly reduced cGAS and STING expression levels in primary adipocytes, interfering with *Hoxa5* expression promoted the activation of the cGAS-STING pathway (Fig. 3E, F). Together with the results of in vivo experiments, this finding

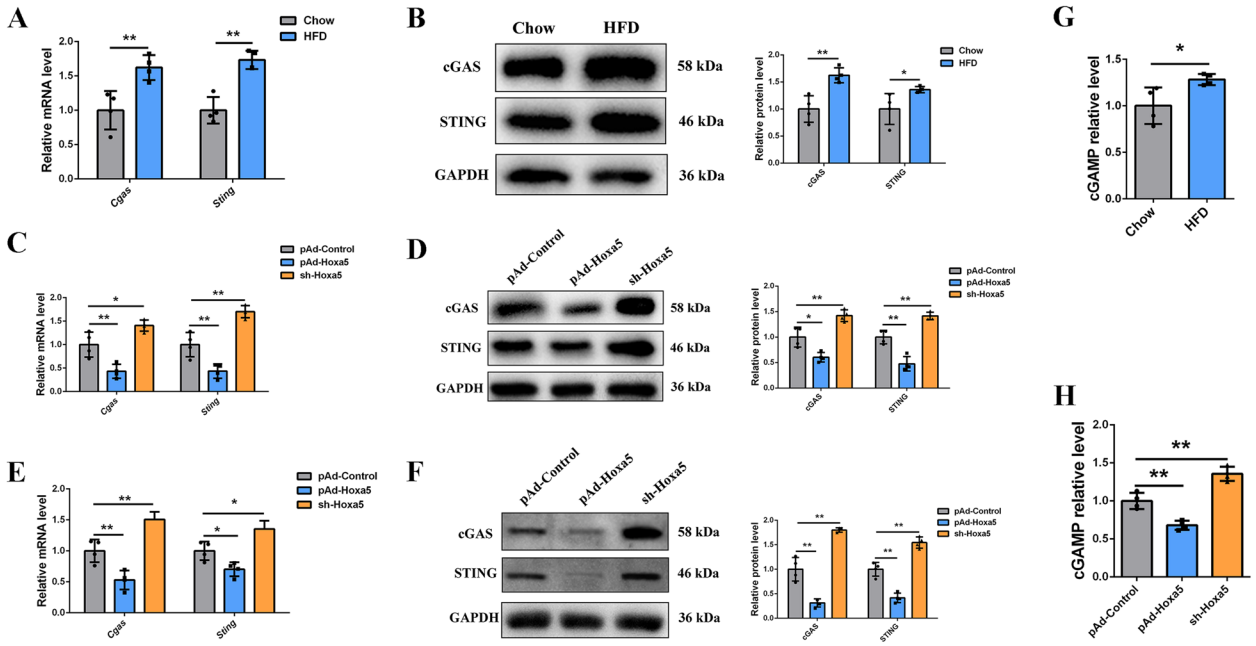

Fig. 3 Hoxa5 inhibits activation of cGAS-cGAMP-STING pathway induced by high-fat diet. **A** iWAT was collected from mice in Chow and HFD groups; *Cgas* and *Sting* were quantified using RT-qPCR. **B** iWAT was collected from mice in Chow and HFD groups; immunoblotting analysis was performed on cGAS (58 kDa) and STING (46 kDa). **C** iWAT was collected from each group of mice after overexpression/interference of *Hoxa5* using adenovirus; *Cgas* and *Sting* were quantified using RT-qPCR. **D** iWAT was collected from each group of mice after overexpression/interference of *Hoxa5* using adenovirus; immunoblotting analysis was performed on cGAS (58 kDa) and STING (46 kDa). **E** Mouse primary adipocytes were treated with palmitic acid after overexpression/interference of Hoxa5; *Cgas* and *Sting* were quantified using RT-qPCR. **F** Mouse primary adipocytes were treated with palmitic acid after overexpression/interference of Hoxa5; immunoblotting analysis was performed on cGAS (58 kDa) and STING (46 kDa). **G** iWAT was collected from mice in Chow and HFD groups; 2′, 3′-cGAMP levels were detected in the supernatants. **H** iWAT was collected from each group of mice after overexpression/interference of *Hoxa5*; 2′, 3′-cGAMP levels were detected in the supernatants. $n = 4$ in each group. Values are mean ± SD. $^{*}p < 0.05$, $^{**}p < 0.01$. iWAT inguinal white adipose tissue, HFD high-fat diet

further suggests that *Hoxa5* is able to inhibit the activation of the cGAS-STING pathway caused by a high-fat diet, which may be related to its ability to reduce MERC production in adipocytes.

In the mammalian immune system, cytoplasmic DNA activates cGAS to synthesize second messenger-cyclic dinucleotides (2′, 3′-cGAMP). cGAMP binds to STING to form a dimer, recruit TBK1, phosphorylate and activate IRF3, induce type I expression of interferons and other cytokines [30]. To validate the activation of the cGAS-STING pathway in adipocytes, we analyzed cGAMP levels (ELISA kit, ARBOR ASSAYS) in iWAT of normal and HFD mice and observed a significant increase in cGAMP levels under high-fat feeding conditions (Fig. 3G). We discovered that overexpression of *Hoxa5* in HFD mice caused a marked reduction in cGAMP levels, while interference with *Hoxa5* resulted in a rise in cGAMP levels (Fig. 3 H). The above results support the notion that the distortion of MERC function due to high-fat diet may be associated with aberrant activation of the cGAS-cGAMP-STING pathway, and that Hoxa5 is able to ameliorate MERC dysfunction while alleviating activation of the STING pathway. However, we may not be able to determine a direct causal relationship between activation of the immune response and increased MERC.

Hoxa5 inhibits the cGAS-STING-TBK1-IRF3 pathway and promotes energy metabolism

TANK-binding kinase 1 (TBK1) is a crucial downstream factor of STING, which serves to phosphorylate the transcription factor IRF3, leading to the transcription of IFN-β and, consequently, activation of the innate immune response [31]. Research suggests that activation of the interferon pathway triggers the production of downstream inflammatory factors and cytokines, which in turn suppress adipocyte thermogenesis and reduce UCP-1 expression [32, 33].

We have found that HFD can lead to structural–functional abnormalities of MERC in adipocytes with concomitant activation of the STING pathway, and therefore, we hypothesize that its mediated innate immune response would further contribute to metabolic disruption in adipose tissue. Comparing the expression levels of TBK1, IRF-3, and UCP-1 in the adipose tissue

of mice fed a normal diet and a high-fat diet (Fig. 4A), we found that HFD-induced activation of the STING pathway led directly to downstream phosphorylation of TBK1 and IRF3, while decreasing the expression of the thermogenic gene UCP-1. After that, we further explored the effect of Hoxa5 on the activation of the TBK1-IRF3 pathway. The findings indicated that upregulation of *Hoxa5* resulted in a marked decrease in the phosphorylation state of TBK1. Conversely, downregulation of *Hoxa5* resulted in a notable increase in the phosphorylation status of TBK1, concomitant with a corresponding alteration in the downstream transcription factor IRF3's phosphorylation level ($p < 0.05$) (Fig. 4B). Meanwhile, the expression of UCP-1 also suggest that *Hoxa5* promoted energy metabolism in adipose tissue (Fig. 4B), which suggests that *Hoxa5* may ameliorate the impaired mitochondrial function caused by HFD, which is closely related to STING pathway activation as well as the function of MERC. Therefore, we examined the expression levels of genes related to mitochondrial genesis and found that overexpression of Hoxa5 significantly promoted mitochondrion generation, whereas interference with Hoxa5 further suppressed mitochondrial function (Fig. 4C).

In order to further confirm the impact of *Hoxa5* on the activation of the STING-TBK1-IRF3 pathway, we treated mouse primary adipocytes in a high-fat environment

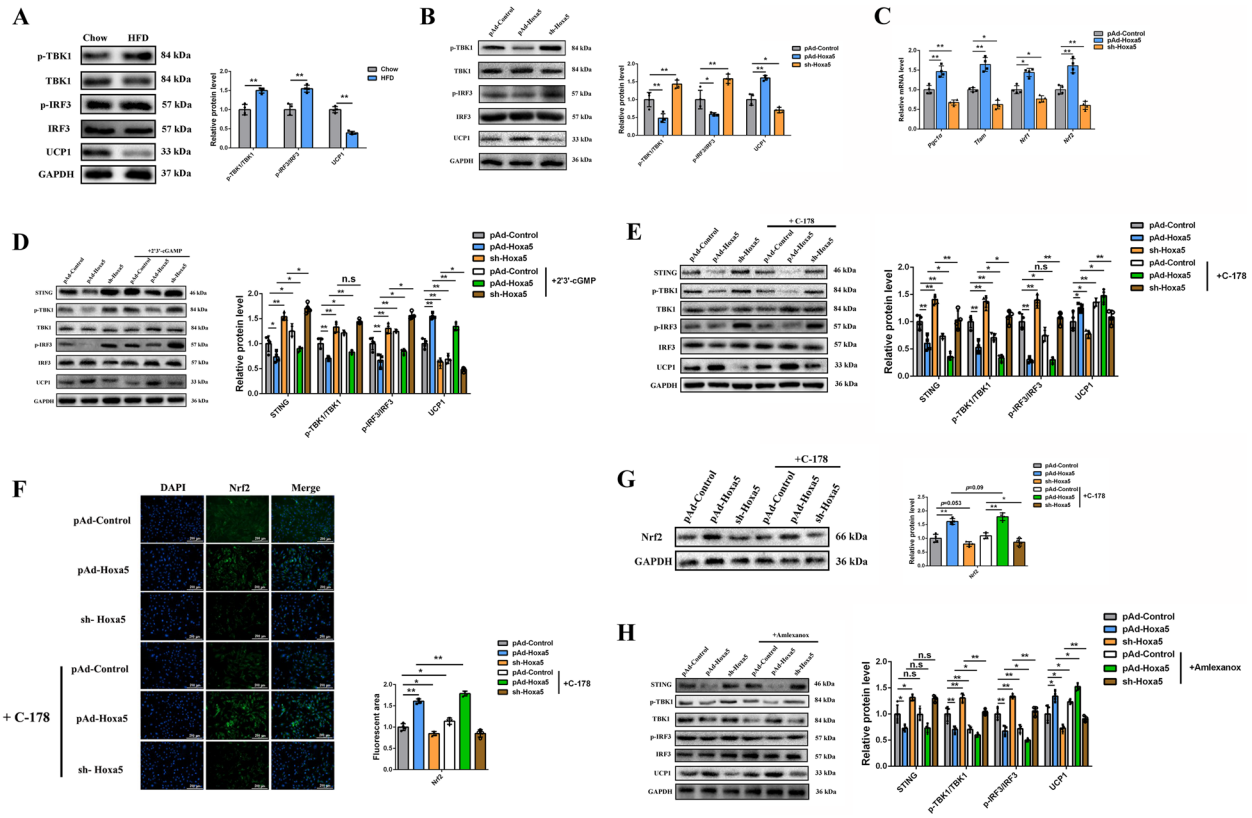

Fig. 4 Hoxa5 inhibits the cGAS-STING-TBK1-IRF3 pathway and promotes energy metabolism. **A** iWAT was collected from mice in Chow and HFD groups; immunoblotting analysis was performed on p-TBK1/TBK1 (84 kDa), p-IRF3/IRF3 (57 kDa), and UCP1 (33 kDa). **B** iWAT was collected from each group of mice after overexpression/interference of *Hoxa5*; immunoblotting analysis was performed on p-TBK1/TBK1 (84 kDa), p-IRF3/IRF3 (57 kDa), and UCP1 (33 kDa). **C** iWAT was collected from each group of mice after overexpression/interference of *Hoxa5*, *Pgc1α*, *Tfam*, *Nrf1*, and *Nrf2* were quantified using RT-qPCR. **D** Mouse primary adipocytes were treated with palmitic acid with the addition of 2′, 3′-cGAMP after overexpression/interference of Hoxa5; immunoblotting analysis was performed on STING (46 kDa), p-TBK1/TBK1 (84 kDa), p-IRF3/IRF3 (57 kDa), and UCP1 (33 kDa). **E** Mouse primary adipocytes were treated with palmitic acid with the addition of C-178 after overexpression/interference of Hoxa5; immunoblotting analysis was performed on STING (46 kDa), p-TBK1/TBK1 (84 kDa), p-IRF3/IRF3 (57 kDa), and UCP1 (33 kDa). **F** Mouse primary adipocytes were treated with palmitic acid with the addition of C-178 after overexpression/interference of Hoxa5, followed by incubation with the NRF2 antibody, labeling by fluorescent secondary antibody followed by imaging by fluorescence microscopy. **G** Mouse primary adipocytes were treated with palmitic acid with the addition of 2′, 3′-cGAMP after overexpression/interference of Hoxa5; immunoblotting analysis was performed on Nrf2 (66 kDa). **H** Mouse primary adipocytes were treated with palmitic acid with the addition of amlexanox after overexpression/interference of Hoxa5; immunoblotting analysis was performed on STING (46 kDa), p-TBK1/TBK1 (84 kDa), p-IRF3/IRF3 (57 kDa), and UCP1 (33 kDa). $n = 4$ in each group. Values are mean ± SD.*$p < 0.05$, **$p < 0.01$. iWAT inguinal white adipose tissue, HFD high fat diet

with the STING activator (2',3'-cGAMP) and inhibitor (C-178), while regulating the expression of *Hoxa5* by overexpression/interference. We discovered a noteworthy increase in STING protein expression and corresponding phosphorylation levels of TBK1 and IRF3 following cGAMP treatment of primary adipocytes. This was accompanied by a significant decrease in the level of UCP-1, which is linked to energy metabolism. Overexpressing *Hoxa5* effectively suppressed STING protein expression and partially hindered STING activation by cGAMP. This resulted in notable reductions in the phosphorylation levels of TBK1 and IRF3 and significant increases in UCP-1 levels. Conversely, inhibition of *Hoxa5* exposure had a contrasting significant effect ($p < 0.05$) (Fig. 4D). Likewise, administration of C-178 exhibited a significant suppression of the TBK1-IRF3 pathway in adipocytes. Whereas overexpression of *Hoxa5* exacerbated the inhibitory effect of C-178, while interference with *Hoxa5* showed the inverse effect ($p < 0.05$) (Fig. 4E). In addition, immunofluorescence experiments as well as immunoblotting showed that supplementation with C-178 or up-regulation of Hoxa5 increased the expression of the mitochondrial biosynthesis gene Nrf2, resulting in improved energy metabolism (Fig. 4F, G).

Subsequently, we administered the TBK1 inhibitor amlexanox to adipocytes and observed a significant reduction ($p < 0.05$) in both TBK1 and IRF3 phosphorylation levels. However, STING expression appeared to be minimally affected, whereas there was a considerable increase ($p < 0.05$) in UCP1 expression. Remarkably, *Hoxa5* overexpression in combination with amlexanox treatment synergistically contributed to decreased phosphorylation levels of TBK1 and IRF3, while also increasing UCP1 expression levels (Fig. 4H).

Hoxa5 alleviates calcium distortions and improves insulin resistance

MERC plays a vital role in cellular homeostasis and can impact insulin sensitivity through multiple pathways such as Ca^{2+} signaling, regulation of lipid metabolism, and maintenance of mitochondrial and endoplasmic reticulum functions [34–36]. Therefore, we attempted to explore the relationship between MERC and calcium homeostasis as well as insulin sensitivity and to uncover the role of Hoxa5 in this regard.

For this purpose, we monitored the body weight of the mice as well as changes in insulin sensitivity. After 7 weeks of being fed a HFD, there was a significant difference ($p < 0.05$) in body weight when compared to the Chow group (Additional file 1: Fig.S2 A). By the tenth week of feeding, significant differences in body size and iWAT size were also observed between mice on different diets (Additional file 1: Fig.S2 B). Furthermore, the outcomes of both the glucose tolerance test (GTT) and insulin tolerance test (ITT) indicated that mice in the HFD group displayed notable impairments in glucose regulation and insulin sensitivity (Additional file 1: Fig. S2 C, D). In addition, we also found that overexpression of *Hoxa5* alleviated insulin resistance caused by a high-fat diet to some extent, whereas the opposite was true for interference with *Hoxa5* (Additional file 1: Fig.S2 E, F). Hoxa5 may also slow down the rate of weight gain in mice, but it did not appear to be significant in the short term (Additional file 1: Fig.S2 G).

AKT is a key molecule in the insulin signaling pathway, and studies have shown that insulin stimulates the recruitment of AKT to MERC and phosphorylation at the Ser473 site [16]. Several MERC-resident proteins are substrates for AKT, including IP3R1 and PACS-2 [37]. Thus, we investigated the alterations in AKT phosphorylation levels in the iWAT of mice and observed a significant decrease in AKT phosphorylation levels in mice of the HFD group ($p < 0.05$). Furthermore, acute insulin stimulation failed to demonstrate a significant increase in AKT phosphorylation levels (Fig. 5A). In contrast, overexpression of *Hoxa5* restored the phosphorylation level of Akt in adipose tissue, while the phosphorylation level of GSK-3β, a key protein downstream of AKT, was significantly increased ($p < 0.01$); whereas interfering with Hoxa5 reduced the basal phosphorylation level of both (Fig. 5B). It is evident that high Hoxa5 expression may alleviate the impairment of insulin signaling caused by HFD.

Insulin sensitivity is closely related to calcium signaling, and studies have shown that obesity may cause an increase in MERC production, which leads to an enhancement of IP3R-VDAC-mediated calcium transport, resulting in a disruption of calcium homeostasis and causing insulin resistance to develop [38, 39]. Therefore, we hypothesized that Hoxa5 may have alleviated insulin resistance in mice by affecting MERC production and IP3R1-VDAC function. Hence, we examined the changes in the protein levels of IP3R1 and VDAC in iWAT after transfection with *Hoxa5* and found that the expression of *Hoxa5* was negatively correlated with the changes in IP3R1-VDAC (Fig. 5C), which was also consistent with the changes in MERC levels. Therefore, we hypothesized that Hoxa5 could regulate intracellular Ca^{2+} flow and alleviate HFD-induced insulin resistance by activating AKT to inhibit the expression and function of IP3R1.

Primary adipocytes were treated with the AKT protein inhibitor KRX-0401 while also undergoing *Hoxa5* overexpression/interference. The results showed that the phosphorylation levels of Akt and GSK-3β were significantly reduced in primary cells after treatment with

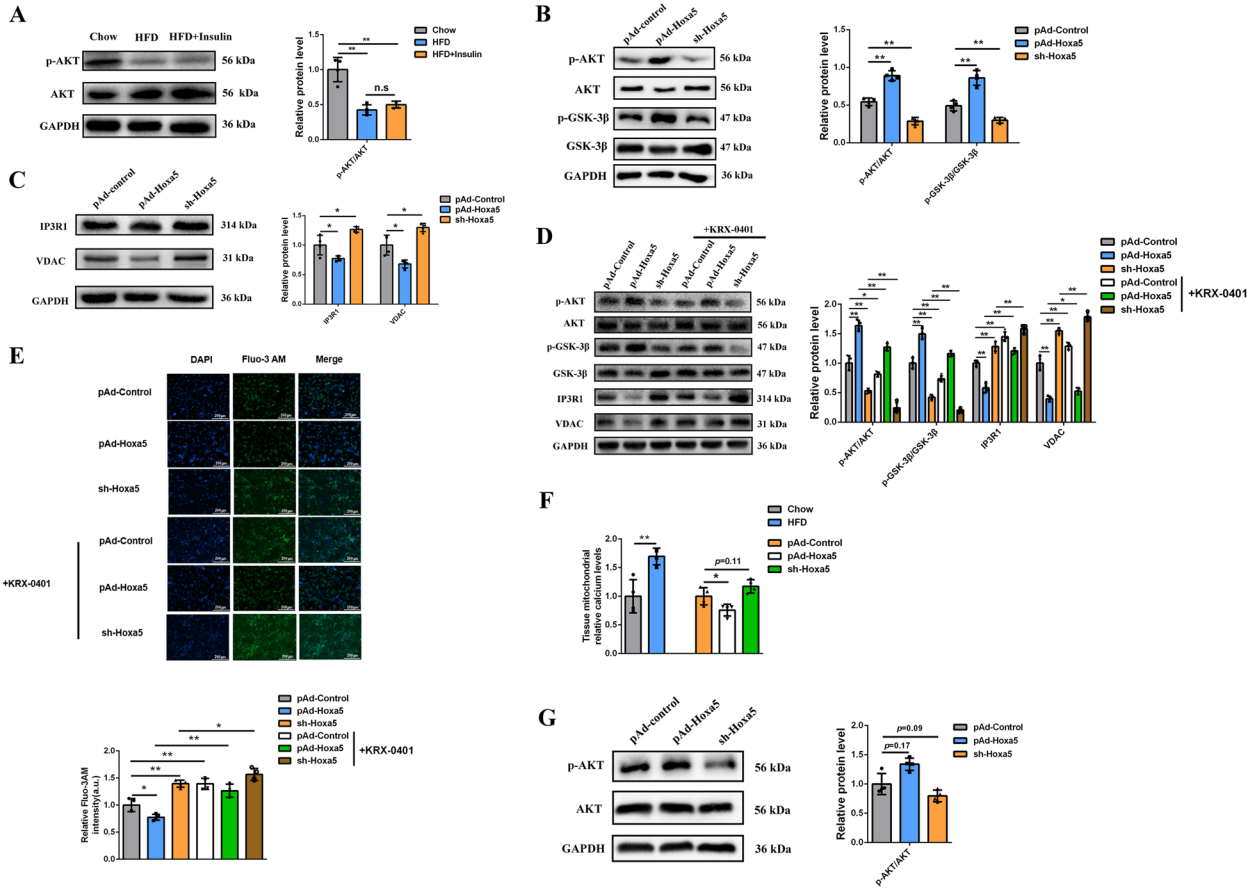

Fig. 5 Hoxa5 alleviates calcium distortions and improves insulin resistance. **A** After 5 h of fasting, insulin (0.5 U/kg) was injected intraperitoneally; after 30 min to collect iWAT, immunoblotting analysis was performed on p-AKT/AKT (56 kDa). **B** iWAT was collected from each group of mice after overexpression/interference of *Hoxa5*; immunoblotting analysis was performed on p-AKT/AKT (56 kDa) and p-GSK-3β/GSK-3β (47 kDa). **C** iWAT was collected from each group of mice after overexpression/interference of *Hoxa5*; immunoblotting analysis was performed on IP3R1 (314 kDa) and VDAC (32 kDa). **D** After overexpression/interference of Hoxa5 on mouse primary adipocytes, the cells were treated with palmitic acid with the addition of KRX-0401; immunoblotting analysis was performed on p-AKT/AKT (56 kDa), p-GSK-3β/GSK-3β (47 kDa), IP3R1 (314 kDa), and VDAC (32 kDa). **E** After overexpression/interference of Hoxa5 on mouse primary adipocytes, the cells were treated with palmitic acid with the addition of KRX-0401, stained with Fluo-3, AM Calcium probe, and visualized using an IFM. **F** The iWAT was collected, mitochondrial fractions were extracted, and Ca^{2+} levels were detected using the tissue intramitochondrial calcium ion concentration fluorescence quantification assay kit, and relative values were calculated by taking the level of mitochondrial protein Cox-2 as an internal reference. **G** Liver was collected from each group of mice after overexpression/interference of Hoxa5; immunoblotting analysis was performed on p-AKT/AKT (56 kDa). $n = 4$ in each group. Values are mean ± SD. *$p < 0.05$, **$p < 0.01$. iWAT inguinal white adipose tissue, HFD high-fat diet, IFM inverted fluorescence microscope

KRX-0401, accompanied by upregulation of IP3R1 and VDAC expression, and to antagonized with overexpression of *Hoxa5*, while synergistic with interference with *Hoxa5* (Fig. 5D). Likewise, fluorescent probe staining for Ca^{2+} illustrates that suppressing the Akt-GSK-3β pathway results in increased levels of cytoplasmic Ca^{2+} (Fig. 5E). In addition, we isolated mitochondrial fractions from iWAT and quantified the levels of Ca^{2+} concentration in mitochondria using the mitochondrial Ca^{2+}-specific fluorescent probe Rhod-2 (tissue intramitochondrial calcium ion concentration fluorescence quantification assay kit, GENMED, USA), further confirming that a HFD increased MERC-mediated Ca^{2+} transport, whereas Hoxa5 decreased calcium accumulation in mitochondria (Fig. 5F).

Moreover, we further examined the effects of Hoxa5 on the changes in the phosphorylation level of Akt in liver tissues and likewise found that Hoxa5 restored the phosphorylation level of AKT to a certain extent (Fig. 5G). Similarly, we examined the effects of serum triglycerides, FFAs, and lipid metabolism genes in iWAT of HFD mice after overexpression/interference of *Hoxa5* and found that increasing the expression level of *Hoxa5* somewhat relieved the adipose tissue and systemic metabolic

distortions (Additional file 1: Fig.S2 H-J). In addition, overexpression of Hoxa5 also led to a decrease in iWAT weight in mice, whereas interference did the opposite, but not significantly (Additional file 1: Fig.S2 K).

Discussion

A significant portion of material exchange among organelles occurs at specialized contact sites on their membranes through interactions between proteins and lipids [40, 41]. The connection between mitochondria and the ER is mediated by proteins at the organelle membrane contact sites, as evidenced by the interference of MERC structure by proteases [42]. As one of the most extensively studied metabolic organelles in cells, the MERC plays a pivotal role in regulating intracellular calcium homeostasis, phospholipid biosynthesis, autophagy, mitochondrial dynamics, apoptosis, and the ER stress response [43, 44]. However, the excessive production of MERC structures may have detrimental effects. Through transmission electron microscopy observations and the use of molecular indicators, our current experiment has confirmed that a high-fat diet can elevate the contact between mitochondria and ER membranes in adipocytes. This elevation is due to an increase in the expression of MERC-associated proteins which can interfere with the normal functioning of MERC, resulting in ER stress. Nevertheless, we have yet to ascertain the precise reason behind the significant elevation in mitochondrial–ER membrane contact resulting from heightened lipid stimulation. This could possibly be an adaptive mechanism employed by the body to counter metabolic distortions by enhancing mitochondrial respiration and reducing lipid accumulation. Ultimately, it results in severe ER stress and insulin resistance.

As a critical transcription factor, HOXA5 plays a pivotal role in regulating various metabolic processes in the body. Previous studies have revealed a significant reduction in *Hoxa5* expression levels in adipocytes when exposed to a HFD [45], indicating its potential involvement in metabolic diseases related to obesity. Recent studies have additionally verified the possible involvement of *Hoxa5*, including its ability to alleviate ER stress by impeding transcriptional activation of the eIF2α/PERK signaling pathway and the PPARγ pathway [46]. Additionally, it facilitates the process of browning white adipose tissue by hindering Tenascin c/Toll-like receptor 4/NFκB inflammatory signaling in mice [47]. Our study investigated the potential mechanism by which *Hoxa5* regulates metabolic distortions induced by high-fat diets, by decreasing the formation of MERC structures in adipocytes. This leads to a reduction in ER stress and disruption of Ca^{2+} homeostasis, thus alleviating the observed metabolic abnormalities. However, the mechanism behind how *Hoxa5* results in a decrease in MERC structure and impacts MERC function remains unclear.

During an intensive exploration of the effect of *Hoxa5* on MERC, we noticed the key role played by STING, which is located in the ER, especially in the MERC structure [48]. Numerous studies in recent years have shown a close connection between STING and the structure and function of MERC. In the presence of relatively weak ER–mitochondrial interactions, MERC may provide a platform for STING to mediate IFN signaling and inflammatory vesicle formation. In contrast, when mitochondrial dynamics are abnormal, higher ER–mitochondrial coupling and calcium exchange may result in STING residing within the Ca^{2+} microdomains of MERC, leading to severe ER stress [49]. Moreover, STING exhibits a close association with metabolic distortions that stem from a high-fat diet. Adipocytes can undergo activation of the cGAS-STING pathway due to mitochondrial stress, leading to an inflammatory response, and insulin resistance [50]. In the present study, we found that MERC dysfunction caused by a high-fat diet may be associated with abnormal activation of the cGAS-cGAMP-STING pathway, while *Hoxa5* may regulate MERC structure and function by affecting intracellular immune responses. Further, *Hoxa5* is also able to inhibit the activation of the TBK1-IRF3 pathway by affecting the cGAS-STING pathway to reduce the occurrence of innate immune responses, thereby affecting mitochondrial function and promoting thermogenesis in adipose tissue. However, we have not yet established a direct causal link between elevated MERC structure and cGAS-STING pathway activation. Additionally, the mechanism by which *Hoxa5* regulates the immune response mediated by MERCs requires further investigation.

Meanwhile, HOXA5 is associated with lipid metabolism as well as insulin sensitivity. Therefore, we further investigated the relationship between merc-mediated regulation of Ca^{2+} homeostasis and insulin sensitivity. In MERC, the Ca^{2+} release channel IP3R and the mitochondrial outer membrane pore protein VDAC form a complex via GRP75 that facilitates the transport of Ca^{2+} from the ER to the mitochondria, which is regulated by a protein complex including AKT kinase and other components [51]. Therefore, we focused on the effect of Hoxa5 on the expression level as well as phosphorylation of AKT and observed the role of the AKT pathway on IP3R1-mediated calcium transport, which explains the regulation of adipose tissue metabolism as well as insulin signaling by the transcription factor HOXA5 from a new perspective. However, we have not yet clarified how HOXA5 acts on the AKT pathway, and although

some studies have shown that HOXA5 can upregulate AKT1 expression or activate the PI3K-AKT pathway, direct evidence is still lacking [52, 53]. Research has also shown that HOXA5 can induce precursor adipose differentiation and alleviate insulin resistance by promoting miR574-5p expression [54]. These findings may help us to explain the functional exercise of in-depth Hoxa5 and also provide a possible direction for us to further explore the mechanism of action of Hoxa5.

In addition, several shortcomings and limitations still exist in our study. For example, GAPDH is commonly used as a housekeeping gene as an internal reference protein in immunoblotting analyses, including some studies related to metabolic distortions [55, 56]. However, in some reports, the expression of GAPDH was affected by metabolic processes [57, 58]. Although we have reassessed that GAPDH expression levels were not significantly affected in our study using *β-actin* as an internal reference, there may still be a potential risk. Additionally, the assessment of the MERC structure by TEM is also affected by the randomness of sample preparation and photographic field of view and could only be referenced as a semi-quantitative result. In subsequent studies, we hope to further precisely quantify the effect of Hoxa5 on MERC formation and related protein interactions using more intuitive methods such as Proximity Ligation Assay (PLA). Furthermore, intuitive dynamic tracking of Ca^{2+} flow between mitochondria and endoplasmic reticulum was also lacking in our study, and relying only on fluorescent staining may have some limitations. Our hope is that a more intuitive calcium tracking method can be used in subsequent studies to accurately assess the calcium exchange problem in MERC.

Conclusions

In summary, our study found that high-fat diet leads to structural and functional dysregulation of MERC in mouse adipocytes, resulting in ER stress and impaired calcium homeostasis, which induces interferon (IFN) responses centered on STING, as well as triggers insulin resistance. Meanwhile, Hoxa5, as an important transcription factor, may affect the expression of MERC-related proteins, thereby reducing MERC production. It may also alleviate metabolic distortions in adipose tissue and insulin resistance by affecting the cGAS-STING pathway and the AKT-IP3R axis, and promote energy metabolism. Our study focused on the relationship between Hoxa5 and MERC, expanding a new pathway for Hoxa5 to regulate the metabolism of adipose tissue, which is expected to be a potential target for the treatment of obesity-related diseases, as well as providing an experimental basis for the refinement of the molecular functional network related to MERC.

Abbreviations

MERC	Mitochondria–endoplasmic reticulum membrane contact
HFD	High-fat diet
Hox	Homeobox
TCA cycle	Tricarboxylic acid cycle
FFAs	Free fatty acids
iWAT	Inguinal white adipose tissue
MERCs	Mitochondria–endoplasmic reticulum membrane contact components
ERs	Endoplasmic reticulum components (ERs)
PMs	Pure mitochondria components
RCs	Residual components
PACS-2	Phosphofurin acidic cluster sorting protein 2
VDAC	Voltage-dependent anion channel protein 1
cGAS	Cyclic GMP-AMP synthase
dsDNA	Double-stranded DNA ()
2′, 3′-cGAMP	Cyclic dinucleotides
TBK1	TANK-binding kinase 1
GTT	Glucose tolerance test
ITT	Insulin tolerance test
IP3Rs	IP3 receptors
RyRs	Ryanodine receptors
IFN	Interferon

Supplementary Information

The online version contains supplementary material available at https://doi.org/10.1186/s12915-024-02047-0.

Additional file 1. Fig. S1. **A** Serum was collected from the Chow and HFD groups of mice, and TG levels in serum were measured using a kit (Nanjing Jiancheng, China); **B** Serum was collected from the Chow and HFD groups of mice, and FFAs levels in serum were measured using a kit (Nanjing Jiancheng, China); **C**, iWAT was collected from mice in Chow and HFD groups, *Fasn*,*Acc1*, *Hsl*, and *Atgl* were quantified using RT-qPCR; **D** iWAT was collected from mice in Chow and HFD groups, immunoblotting analysis was performed on HOXA5 (29 kDa); **E** iWAT was collected from mice in Chow and HFD groups, *Hoxa5* were quantified using RT-qPCR; **F** iWAT was collected from mice after overexpression/interference of *Hoxa5*,immunoblotting analysis was performed on HOXA5 (29 kDa); **G** iWAT was collected from mice after overexpression/interference of *Hoxa5*, *Hoxa5* were quantified using RT-qPCR; **H** After overexpression/interference of *Hoxa5*, *Hoxa5* were quantified using RT-qPCR in liver, eWAT and BAT; **I** After enrichment of the MERC fraction, immunoblot analysis of PACS-2 (130 kDa) and VDAC (32 kDa) in each fraction was performed; **J** iWAT was collected from mice in Chow and HFD groups, *Ip3r1* were quantified using RT-qPCR; **K** iWAT was collected from mice after overexpression/interference of *Hoxa5*, *Ip3r1* were quantified using RT-qPCR; **L** After palmitic acid treatment of primary adipocytes, *Chop*, *Grp78* and *Ire1a* were quantified using RT-qPCR; **M** Mouse primary adipocytes were treated with palmitic acid after overexpression/interference of Hoxa5, *Chop*,*Grp78* and *Ire1a* were quantified using RT-qPCR. $n = 4$ in each groups, Values are mean±SD. * $p<0.05$, ** $p<0.01$. HFD, high fat diet; TG, triglyceride; FFAs, free fatty acids; iWAT, inguinal white adipose tissue; MERCs, mitochondria-endoplasmic reticulum membrane contact components; ERs, endoplasmic reticulum components; PMs, pure mitochondria components; RCs, residual components. eWAT, epididymal white adipose tissue; BAT, brown adipose tissu

Additional file 2. Fig. S2. **A** Changes in body weight of Chow and HFD groups of mice during 13 weeks of feeding a high-fat diet (60% fat for energy); **B** Comparison of body size (left) and iWAT size (right) between Chow and HFD groups of mice after 13 weeks of feeding; **C** After 16 h of fasting, mice were injected intraperitoneally with glucose (1.5 g/kg), and tail-vein blood glucose levels were measured with a glucometer before (0 min) and 15, 30, 45, 60, 90, and 120 min after injection; **D** After 5 h of fasting, mice were injected intraperitoneally with insulin (0.4 U/kg), and tail-vein blood glucose levels were measured with a glucometer before (0 min) and 15, 30, 45, 60, 90, and 120 min after injection; **E** Glucose tolerance test in mice after overexpression/disruption of Hoxa5;**F** Insulin

tolerance testing of mice after overexpression/disruption of Hoxa5; **G** Changes in body weight of mice in each group during overexpression/interference with Hoxa5;**H** Mice serum was collected after overexpression/interference with Hoxa5, TG levels in serum were measured using a kit (Nanjing Jiancheng, China); **I** Mice serum was collected after overexpression/interference with Hoxa5, FFAs levels in serum were measured using a kit (Nanjing Jiancheng, China); **J** iWAT was collected from each group of mice after overexpression/interference of *Hoxa5*,*Fasn*, *Acc1*, *Hsl*, and *Atgl* were quantified using RT-qPCR;**K** Relative change in iWAT weight (two articles)/weight ratio. $n = 4$ in each groups, Values are mean±SD. * $p<0.05$, ** $p<0.01$. HFD, high fat diet; TG, triglyceride; FFAs, free fatty acids; iWAT, inguinal white adipose tissue

Acknowledgements
Not applicable.

Authors' contributions
Qi Chen: conceptualization, methodology, and writing—original draft; Zeyu Ren: formal analysis and software. Liping Dang: writing—reviewing and editing. Zunhai Liu and Simeng Wang: data curation. Xinhao Chen and Guiping Qiu: visualization. Chao Sun: design and supervision. All authors read and approved the final manuscript.

Funding
This study was supported by National Key Research and Development Program of China (2021YFF1000602) and the Major National Scientific Research Projects (2015CB943102).

Data availability
All data generated or analyzed during this study are included in this published article and its supplementary information files.

Declarations

Ethics approval and consent to participate
All animal experiments were conducted in accordance with the Animal Ethics Committee (Northwest Agriculture and Forestry University, Yangling, Shaanxi, China).

Consent for publication
Not applicable.

Competing interests
The authors declare no conflict of interest.

Received: 5 September 2023 Accepted: 16 October 2024
Published online: 29 October 2024

References

1. Via MA, Mechanick JI. Obesity as a disease. Curr Obes Rep. 2014;3(3):291–7.
2. Thesleff I. Homeobox genes and growth factors in regulation of craniofacial and tooth morphogenesis. Acta Odontol Scand. 1995;53(3):129–34.
3. Seifert A, Werheid DF, Knapp SM, Tobiasch E. Role of Hox genes in stem cell differentiation. World J Stem Cells. 2015;7(3):583–95.
4. Gesta S, Blüher M, Yamamoto Y, et al. Evidence for a role of developmental genes in the origin of obesity and body fat distribution. Proc Natl Acad Sci U S A. 2006;103(17):6676–81.
5. Passaro A, Miselli MA, Sanz JM, et al. Gene expression regional differences in human subcutaneous adipose tissue. BMC Genomics. 2017;18(1):202.
6. Cao W, Xu Y, Luo D, Saeed M, Sun C. Hoxa5 promotes adipose differentiation via increasing DNA methylation level and inhibiting PKA/HSL signal pathway in mice. Cell Physiol Biochem. 2018;45(3):1023–33.
7. Holzman MA, Ryckman A, Finkelstein TM, et al. HOXA5 participates in brown adipose tissue and epaxial skeletal muscle patterning and in brown adipocyte differentiation. Front Cell Dev Biol. 2021;9: 632303.
8. Parrillo L, Costa V, Raciti GA, et al. Hoxa5 undergoes dynamic DNA methylation and transcriptional repression in the adipose tissue of mice exposed to high-fat diet. Int J Obes (Lond). 2016;40(6):929–37.
9. Franke WW, Kartenbeck J. Outer mitochondrial membrane continuous with endoplasmic reticulum. Protoplasma. 1971;73(1):35–41.
10. Morré DJ, Merritt WD, Lembi CA. Connections between mitochondria and endoplasmic reticulum in rat liver and onion stem. Protoplasma. 1971;73(1):43–9.
11. Vance JE. Phospholipid synthesis in a membrane fraction associated with mitochondria. J Biol Chem. 1990;265(13):7248–56.
12. Csordás G, Várnai P, Golenár T, et al. Imaging interorganelle contacts and local calcium dynamics at the ER-mitochondrial interface. Mol Cell. 2010;39(1):121–32.
13. García-Pérez C, Hajnóczky G, Csordás G. Physical coupling supports the local Ca2+ transfer between sarcoplasmic reticulum subdomains and the mitochondria in heart muscle. J Biol Chem. 2008;283(47):32771–80.
14. Rizzuto R, Duchen MR, Pozzan T. Flirting in little space: the ER/mitochondria Ca2+ liaison. Sci STKE. 2004;2004(215):re1.
15. Puglielli L, Konopka G, Pack-Chung E, et al. Acyl-coenzyme A: cholesterol acyltransferase modulates the generation of the amyloid beta-peptide. Nat Cell Biol. 2001;3(10):905–12.
16. Tubbs E, Theurey P, Vial G, et al. Mitochondria-associated endoplasmic reticulum membrane (MAM) integrity is required for insulin signaling and is implicated in hepatic insulin resistance. Diabetes. 2014;63(10):3279–94.
17. Sebastián D, Hernández-Alvarez MI, Segalés J, et al. Mitofusin 2 (Mfn2) links mitochondrial and endoplasmic reticulum function with insulin signaling and is essential for normal glucose homeostasis. Proc Natl Acad Sci U S A. 2012;109(14):5523–8.
18. Pan M, Sun Q, Li C, Tai R, Shi X, Sun C. Hoxa5 inhibits adipocyte proliferation through transcriptional regulation of Ccne1 and blocking JAK2/STAT3 signaling pathway in mice. Biochem Cell Biol. 2022;100(4):325–37.
19. Rong B, Wu Q, Reiter RJ, Sun C. The mechanism of oral melatonin ameliorates intestinal and adipose lipid dysmetabolism through reducing Escherichia coli-derived lipopolysaccharide. Cell Mol Gastroenterol Hepatol. 2021;12(5):1643–67.
20. Hayashi T, Rizzuto R, Hajnoczky G, Su TP. MAM: more than just a housekeeper. Trends Cell Biol. 2009;19(2):81–8.
21. Bravo R, Vicencio JM, Parra V, et al. Increased ER-mitochondrial coupling promotes mitochondrial respiration and bioenergetics during early phases of ER stress. J Cell Sci. 2011;124(Pt 13):2143–52.
22. Kumar V, Maity S. ER Stress-sensor proteins and ER-mitochondrial cross-talk-signaling beyond (ER) stress response. Biomolecules. 2021;11(2):173.
23. Gottschalk B, Koshenov Z, Bachkoenig OA, Rost R, Malli R, Graier WF. MFN2 mediates ER-mitochondrial coupling during ER stress through specialized stable contact sites. Front Cell Dev Biol. 2022;10: 918691.
24. Hayashi T, Su TP. Sigma-1 receptor chaperones at the ER-mitochondrion interface regulate Ca(2+) signaling and cell survival. Cell. 2007;131(3):596–610.
25. Du H, Xu T, Cui M. cGAS-STING signaling in cancer immunity and immunotherapy. Biomed Pharmacother. 2021;133: 110972.
26. Ran JS, Jin J, Zhang XX, et al. Molecular characterization, expression and functional analysis of chicken STING. Int J Mol Sci. 2018;19(12):3706.
27. Wu J, Chen YJ, Dobbs N, et al. STING-mediated disruption of calcium homeostasis chronically activates ER stress and primes T cell death. J Exp Med. 2019;216(4):867–83.
28. Ma XM, Geng K, Law BY, et al. Lipotoxicity-induced mtDNA release promotes diabetic cardiomyopathy by activating the cGAS-STING pathway in obesity-related diabetes. Cell Biol Toxicol. 2023;39(1):277–99.
29. Hu H, Zhao R, He Q, et al. cGAS-STING mediates cytoplasmic mitochondrial-DNA-induced inflammatory signal transduction during accelerated senescence of pancreatic β-cells induced by metabolic stress. FASEB J. 2022;36(5): e22266.
30. Wei X, Zhang L, Yang Y, et al. LL-37 transports immunoreactive cGAMP to activate STING signaling and enhance interferon-mediated host antiviral immunity. Cell Rep. 2022;39(9): 110880.
31. Zhao B, Du F, Xu P, et al. A conserved PLPLRT/SD motif of STING mediates the recruitment and activation of TBK1. Nature. 2019;569(7758):718–22.

32. Bai J, Cervantes C, He S, et al. Mitochondrial stress-activated cGAS-STING pathway inhibits thermogenic program and contributes to overnutrition-induced obesity in mice. Commun Biol. 2020;3(1):257.
33. Hoang AC, Sasi-Szabó L, Pál T, et al. Mitochondrial RNA stimulates beige adipocyte development in young mice. Nat Metab. 2022;4(12):1684–96.
34. Rieusset J. The role of endoplasmic reticulum-mitochondria contact sites in the control of glucose homeostasis: an update. Cell Death Dis. 2018;9(3):388.
35. Ma X, Qian H, Chen A, Ni HM, Ding WX. Perspectives on mitochondria-ER and mitochondria-lipid droplet contact in hepatocytes and hepatic lipid metabolism. Cells. 2021;10(9):2273.
36. Ziegler DV, Martin N, Bernard D. Cellular senescence links mitochondria-ER contacts and aging. Commun Biol. 2021;4(1):1323.
37. Betz C, Stracka D, Prescianotto-Baschong C, Frieden M, Demaurex N, Hall MN. Feature article: mTOR complex 2-Akt signaling at mitochondria-associated endoplasmic reticulum membranes (MAM) regulates mitochondrial physiology. Proc Natl Acad Sci U S A. 2013;110(31):12526–34.
38. Thoudam T, Ha CM, Leem J, et al. PDK4 augments ER-mitochondria contact to dampen skeletal muscle insulin signaling during obesity. Diabetes. 2019;68(3):571–86.
39. Beaulant A, Dia M, Pillot B, et al. Endoplasmic reticulum-mitochondria miscommunication is an early and causal trigger of hepatic insulin resistance and steatosis. J Hepatol. 2022;77(3):710–22.
40. Gatta AT, Levine TP. Piecing together the patchwork of contact sites. Trends Cell Biol. 2017;27(3):214–29.
41. Prinz WA. Bridging the gap: membrane contact sites in signaling, metabolism, and organelle dynamics. J Cell Biol. 2014;205(6):759–69.
42. Shiao YJ, Balcerzak B, Vance JE. A mitochondrial membrane protein is required for translocation of phosphatidylserine from mitochondria-associated membranes to mitochondria. Biochem J. 1998;331(Pt 1):217–23.
43. Vance JE. MAM (mitochondria-associated membranes) in mammalian cells: lipids and beyond. Biochim Biophys Acta. 2014;1841(4):595–609.
44. Naon D, Scorrano L. At the right distance: ER-mitochondria juxtaposition in cell life and death. Biochim Biophys Acta. 2014;1843(10):2184–94.
45. Yamamoto Y, Gesta S, Lee KY, Tran TT, Saadatirad P, Kahn CR. Adipose depots possess unique developmental gene signatures [published correction appears in Obesity (Silver Spring). 2010 May;18(5):1064]. Obesity (Silver Spring). 2010;18(5):872–878.
46. Cao W, Zhang T, Feng R, et al. Hoxa5 alleviates obesity-induced chronic inflammation by reducing ER stress and promoting M2 macrophage polarization in mouse adipose tissue. J Cell Mol Med. 2019;23(10):7029–42.
47. Cao W, Huang H, Xia T, Liu C, Muhammad S, Sun C. Homeobox a5 promotes white adipose tissue browning through inhibition of the tenascin C/Toll-like receptor 4/nuclear factor kappa B inflammatory signaling in mice. Front Immunol. 2018;9:647.
48. Luan Y, Luan Y, Yuan RX, Feng Q, Chen X, Yang Y. Structure and function of mitochondria-associated endoplasmic reticulum membranes (MAMs) and their role in cardiovascular diseases. Oxid Med Cell Longev. 2021;2021:4578809.
49. Xue C, Dong N, Shan A. Putative role of STING-mitochondria associated membrane crosstalk in immunity. Trends Immunol. 2022;43(7):513–22.
50. Bai J, Cervantes C, Liu J, et al. DsbA-L prevents obesity-induced inflammation and insulin resistance by suppressing the mtDNA release-activated cGAS-cGAMP-STING pathway. Proc Natl Acad Sci U S A. 2017;114(46):12196–201.
51. Li Y, Chen D, Xu J, Wang X, Zhou F. The spatial expression of mTORC2-AKT-IP3R signal pathway in mitochondrial combination of endoplasmic reticulum of maternal fetal interface trophoblast in intrahepatic cholestasis of pregnancy. J Perinat Med. 2023;51(8):1032–9.
52. Kim CY, Kim YC, Oh JH, Kim MH. HOXA5 confers tamoxifen resistance via the PI3K/AKT signaling pathway in ER-positive breast cancer. J Cancer. 2021;12(15):4626–37.
53. Arderiu G, Cuevas I, Chen A, Carrio M, East L, Boudreau NJ. HoxA5 stabilizes adherens junctions via increased Akt1. Cell Adh Migr. 2007;1(4):185–95.
54. Li Y, Li J, Yu H, et al. HOXA5-miR-574-5p axis promotes adipogenesis and alleviates insulin resistance. Mol Ther Nucleic Acids. 2021;27:200–10.
55. Kuang J, Wang J, Li Y, et al. Hyodeoxycholic acid alleviates non-alcoholic fatty liver disease through modulating the gut-liver axis. Cell Metab. 2023;35(10):1752–1766.e8.
56. Jiang X, Fulte S, Deng F, et al. Lack of VMP1 impairs hepatic lipoprotein secretion and promotes non-alcoholic steatohepatitis. J Hepatol. 2022;77(3):619–31.
57. Kanwar M, Kowluru RA. Role of glyceraldehyde 3-phosphate dehydrogenase in the development and progression of diabetic retinopathy. Diabetes. 2009;58(1):227–34.
58. Dugail I, Quignard-Boulange A, Bazin R, Le Liepvre X, Lavau M. Adipose-tissue-specific increase in glyceraldehyde-3-phosphate dehydrogenase activity and mRNA amounts in suckling pre-obese Zucker rats. Effect of weaning [published correction appears in Biochem J 1989 Feb 1;257(3):following 934]. Biochem J. 1988;254(2):483–487.

Publisher's Note